Chaos: A new mechanism for enhancing the optical generation rate in optically thin solar cells

Cite as: Chaos **29**, 093132 (2019); https://doi.org/10.1063/1.5111042
Submitted: 22 May 2019 . Accepted: 06 September 2019 . Published Online: 30 September 2019

E. Seim, A. Kohler, R. Lukacs, M. A. Brandsrud, E. S. Marstein, E. Olsen, and R. Blümel

Chaos: A new mechanism for enhancing the optical generation rate in optically thin solar cells

Cite as: Chaos **29**, 093132 (2019); doi: 10.1063/1.5111042
Submitted: 22 May 2019 · Accepted: 6 September 2019 ·
Published Online: 30 September 2019

E. Seim,[1,a)] A. Kohler,[1] R. Lukacs,[1] M. A. Brandsrud,[1] E. S. Marstein,[2,3] E. Olsen,[1] and R. Blümel[4]

AFFILIATIONS

[1]RealTek, Norwegian University of Life Sciences, Ås 1430, Norway
[2]Department of Solar Energy, Institute of Energy Technology, Kjeller 2007, Norway
[3]Department of Technology Systems, University of Oslo, Oslo 0371, Norway
[4]Department of Physics, Wesleyan University, Middletown, CT 06457, USA

[a)]e.seim.es@gmail.com

ABSTRACT

The photogenerated current of solar cells can be enhanced by light management with surface structures. For solar cells with optically thin absorbing layers, it is especially important to take advantage of this fact through light trapping. The general idea behind light trapping is to use structures, either on the front surface or on the back, to scatter light rays to maximize their path length in the absorber. In this paper, we investigate the potential of chaotic scattering for light trapping. It is well known that the trajectories close to the invariant set of a chaotic scatterer spend a very long time inside of the scatterer before they leave. The invariant set, also called the chaotic repeller, contains all rays of infinite length that never enter or leave the region of the scatterer. If chaotic repellers exist in a system, a chaotic dynamics is present in the scatterer. As a model system, we investigate an elliptical dome structure placed on top of an optically thin absorbing film, a system inspired by the chaotic Bunimovich stadium. A classical ray-tracing program has been developed to classify the scattering dynamics and to evaluate the absorption efficiency, modeled with Beer-Lambert's law. We find that there is a strong correlation between the enhancement of absorption efficiency and the onset of chaotic scattering in such systems. The dynamics of the systems was shown to be chaotic by their positive Lyapunov exponents and the noninteger fractal dimension of their scattering fractals.

Chaotic scattering of light rays is a feature of many types of surface-structured solar cells. Scattering structures that lead to chaotic scattering have an invariant set of infinitely long-lived trajectories. In this paper, we illustrate how concepts and methods from the field of chaos can provide valuable insights for further developments in a vastly different field: light management in optically thin solar cells.

I. INTRODUCTION

Photovoltaic solar cells (PV) are an increasingly important source of renewable energy. In order to increase the competitiveness of solar electricity, it is desirable to reduce the material costs of solar cells and modules further. Thin solar cells are less prone to bulk recombination and can exhibit larger voltages than their thicker counterparts. In addition, they require less absorber materials, which can reduce cost and environmental footprint further. Reducing the thickness of solar cells requires low surface recombination, as well as an efficient light-trapping scheme to avoid excessive transmission and/or reflection losses. Silicon-based solar cells represent by far the most widespread solar cell technology today. However, silicon exhibits an indirect electronic band gap, which results in weak absorption. This makes the development of surface structures with efficient light-trapping properties even more important for thin silicon solar cells. Additionally, commercial silicon-based PV production has become so refined that the theoretical maximal efficiency of 29.8%[1] might soon be a limiting factor. This further motivates to look to more efficient alternatives like thin film PV.

A number of different mechanisms for absorption efficiency enhancement are discussed in the scientific literature and some

of them are already implemented in solar cell technology. These efforts range from plasmonics[2] to surface-structured light-trapping designs with either ordered structures or random surfaces.[3–9] In light-trapping designs, the aim is to establish surface structures that keep as many of the incoming light rays as long as possible in the absorber. This maximizes the chance of absorption before the rays can leave the solar cell. The maximal enhancement factor for intensity with respect to the incident intensity is $4n^2$, where n is the index of refraction of the solar cell, a limit shown by Yablonovitch in 1982, commonly called the Yablonovitch limit.[10] To show this, Yablonovitch theorized that a truly random surface texture applied to both sides of a film would randomize the direction of the rays interacting with the surface, thus effectively trapping the light rays by maximizing the chance of total internal reflection to occur.

Ray trapping is a phenomenon that has been extensively investigated in the context of chaotic scattering systems. Chaotic scattering systems have been studied for quantum wave systems and the corresponding classical ray systems, and several textbooks have been published in this field.[11–13] Chaos is a mature field of research with a rich set of tools to study dynamics both classically, using rays, and quantum mechanically, using waves. Chaotic systems were originally studied by Henri Poincaré, who investigated the three-body problem in the 1890s.[14] In the 1960s, Lorenz modeled the atmosphere for weather prediction using three coupled nonlinear ordinary differential equations.[15] The famous butterfly effect originates from this work. Both Poincaré and Lorenz found systems that exhibit extreme sensitivity to the initial conditions. The study of dynamical billiards started in 1898 when Hadamard showed that all trajectories in a Hadamard billiard diverge exponentially, thus proving for the first time the existence of what nowadays is called "deterministic chaos" in a dynamical system.[16] Later, in the 1970s and 1980s, Bunimovich also studied dynamical billiards and proved that the dynamics of the "Bunimovich stadium," a special dynamical billiard [Fig. 1(a)],[17–19] is chaotic. The class of dynamical billiards that is important for this work are those where we consider a frictionless particle (a model photon) moving on a flat surface in the presence of some additional structures that reflect, transmit, and refract the particle, akin to the dynamics in a dielectric cavity,[20,21] such as the dielectric-loaded Bunimovich stadium.[22] Chaotic scattering systems were for the first time studied in the late 1980s. By the early 1990s, many different chaotic scattering systems had been studied;[23] three-disk scattering,[24] celestial mechanics,[25,26] charged-particle trajectories in electric and magnetic fields,[27] and scattering in atomic and nuclear physics,[28–30] to name only a few. A review of new developments was written by Seoane and Sanjuán.[31]

In this study, we investigate if chaotic scattering can be considered as a mechanism for absorption enhancement and eventually used as a guide for designing efficient solar cell surfaces for thin solar cells. As a model system, we use a dome structure consisting of half an ellipse and a rectangular slab mimicking the solar cell absorber. The shape chosen is similar to the dielectric-loaded Bunimovich stadium,[22] which is a stadium that is cut in half along the middle of the long side. We call our model system film + dome. The film + dome system has mirrors at the bottom and on the sides. The model system we have chosen is thus a model for dome-shaped surface-structured solar cells. This is a two-dimensional model, but we imagine a third dimension, orthogonal to the two-dimensional plane of our model, in which our two-dimensional model is continued with cylindrical symmetry. Thus, our two-dimensional model reflects the dynamics of the three-dimensional cylindrically symmetric system on a cut orthogonal to its cylinder axis. There are two ray-splitting surfaces present; the elliptical air-dome interface and the flat dome-film interface.

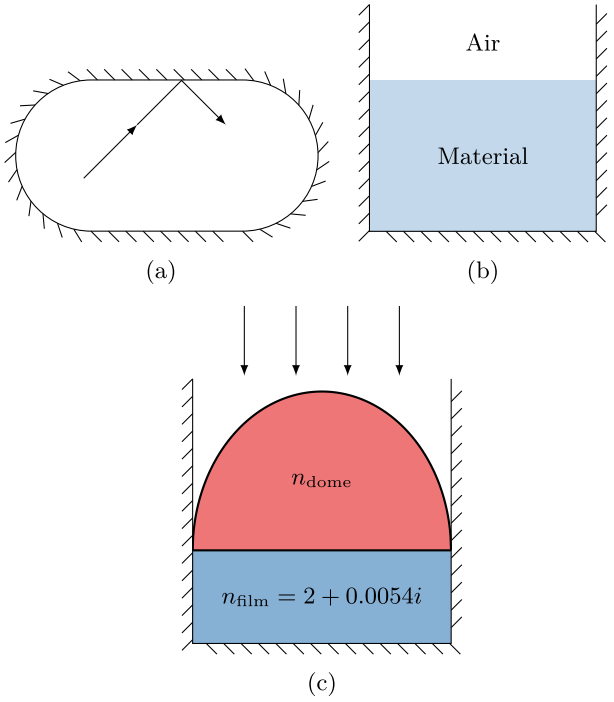

FIG. 1. (a) The Bunimovich stadium is a dynamical billiard extensively studied in the context of chaos. (b) The open system is comprised of three mirrors arranged in a bucketlike shape. The energy converting material in a solar cell can be modeled by a complex refractive index. (c) A 3.46 μm tall dome on top of a 2 μm thick film. The width of the film and dome is 5 μm. The arrows show how incident rays are sent toward the surface.

Outside of the film + dome, the refractive index is equal to one. Ray-splitting systems have been extensively studied in the field of quantum chaos.[32–38] In ray-splitting systems, rays impinging on the surface of the film + dome are transmitted and reflected according to probabilities, which in electrodynamics are calculated by the Fresnel equations.

Since the mechanisms of chaos have to our knowledge so far attracted very little attention in the context of absorption enhancement,[39] we start this paper with a brief account of classical chaos, highlighting aspects of chaos of relevance for the understanding of this paper. We then introduce our classical ray-tracing model for studying dynamical scattering systems. We demonstrate and discuss the relevance of chaos in the context of absorption enhancement due to surface structuring of solar cells. Finally, we compare our classical ray-tracing simulations with finite difference time domain (FDTD) electromagnetic (E&M) wave calculations.

II. CLASSICAL CHAOS

Chaotic dynamical systems are extremely sensitive to initial conditions. In practice, this means that although chaotic systems are governed by purely deterministic laws, they do not have closed-form solutions. Lorenz puts it this way: "Chaos: When the present determines the future, but the approximate present does not approximately determine the future," which expresses the fact that while the classical dynamics of deterministic chaos is in principle predictable, small deviations lead to a completely different dynamics. The sensitivity to initial conditions can be quantified by the Lyapunov exponent. Consider two rays started from almost the same initial conditions in phase space. If the rays are started from and evolve in a chaotic region in phase space, they will, after some point in time, evolve on dramatically different trajectories. Before this happens, the two rays will diverge exponentially fast away from each other. The Lyapunov exponent is a measure of the rate of this divergence. It is given as

$$s(t) = e^{\lambda t} s(0), \tag{1}$$

where λ is the Lyapunov exponent, $s(0)$ is the initial separation distance in phase space, and $s(t)$ is the separation at a time t. A positive Lyapunov exponent means that the divergence is exponentially fast. Thus, a positive Lyapunov exponent is a signature of classical chaos. The separation at $t \neq 0$ can be measured in a Poincaré surface of section (PSOS), which is a section of the total phase space. A PSOS may be used as a way to visualize a trajectory via an intersection surface in physical space.

In dynamical billiards and scattering systems, rays can follow periodic trajectories, also called periodic orbits. However, in scattering systems, periodic orbits can never escape the system; otherwise, they would not be periodic. These rays make up a part of the invariant set of infinitely long-lived trajectories; the other part is made up of nonescaping, nonperiodic trajectories.[40,41] The geometry of the invariant set can be visualized in phase space. If the invariant set has a fractal geometric structure in phase space, it is a sign of sensitivity with respect to initial conditions, thus a sign of chaos. Fractal invariant sets in scattering systems are also called chaotic repellers. It is known that when a trajectory is started near a chaotic repeller, it takes a very long time to move away from the chaotic repeller when the phase space is a mix of chaotic and regular regions.[42]

The notion of fractals and fractal dimensions was first discussed by Mandelbrot in 1967, although the actual terms were introduced later, in 1975.[43] The fractal dimension of the invariant set can be found using a standard method called box counting,[44,45] which we will also use in our paper to estimate the fractal dimension of the phase space. The procedure is to cover the phase space with boxes and count how many boxes contain parts of the invariant set at different scales. We define the fractal dimension d as

$$d = \lim_{M \to \infty} \frac{\log N}{\log M}, \tag{2}$$

where N is the number of boxes that contain a part of the invariant set at a scale M. In a numerical approximation of d, however, M is finite.

III. A MODEL FOR STUDYING CHAOS

A solar cell is a scattering system. Electromagnetic radiation enters the system and may be completely or partially absorbed. We may describe the electromagnetic radiation and its interaction with a solar cell by a ray model in the following way. Light rays enter the solar cell through the front surface. Light that is not absorbed may be reflected from the metallic back contacts and eventually leave the solar cell. The absorption of electromagnetic radiation by the solar cell can be taken into account by associating the rays with amplitudes that are decreasing according to the attenuation described by the Beer-Lambert law. In this paper, we simulate a solar cell by introducing a model system with a defined geometry and enclosing it in a "bucket" of perfect mirrors, see Fig. 1(b). With this constraint, the rays can only leave through the front side. Although real mirrors have some degree of absorption and transmission, we neglect these effects in our simulations and, for the sake of simplicity, treat all mirrors in our simulations as perfect mirrors. In our open bucket, we study chaotic and regular ray dynamics with the help of classical ray tracing and use our simulations to compare systems exhibiting chaotic phase-space structures with systems exhibiting more regular phase-space structures.

It is known that circular, rectangular, and triangular billiards are regular systems with no chaotic dynamics. However, introducing a stepped potential inside such billiards produces chaos.[46,47] This is analogous to placing a material with an index of refraction larger than 1 in our mirror bucket. Our model system, which we place in the bucket, is a structure comprised of a flat film with a dome placed on top as seen in Fig. 1(c). The dome structure is half an ellipse and the film is a rectangular slab. The shape is similar to a Bunimovich stadium cut in half along the middle of the long side, which, similar to our ellipses, has semicircles attached to its rectangular middle section. We name our model system film + dome. We explore film + dome systems, where we keep the refractive index in the film at a constant value of $n_{\text{film}} = 2 + 0.0054i$ and vary the refractive index in the dome n_{dome} to look for a transition from regular to chaotic scattering dynamics. The imaginary part of n_{film} is chosen to be the same value as for silicon at 800 nm,[48] truncated to four decimals. Silicon is not a very good light absorber at this wavelength. Thus, the value is a good choice when looking to improve absorption properties.

A. Classical ray tracing

In principle, if properly equipped with phases, Maxwell's equations may be solved exactly using classical rays. We illustrated this wave-ray equivalence recently by solving the wave equation of a one-dimensional, dissipative, and layered solar cell exactly with the help of classical rays that were properly equipped with phases.[49] An equivalently exact ray-tracing theory for two-dimensional dissipative systems has not yet been described. However, in the geometric-optic limit, where the wavelength is small compared to the scattering structures, it is common practice in the literature to consider optical rays. Following this practice, we will use a classical ray-tracing approach, neglecting proper inclusion of phases. Since we know that the inclusion of phases is essential to obtain a one-to-one correspondence with Maxwell's equations, we accept that our results are approximations. However, quantities computed as averages over ensembles of rays

may still be quite accurate, since statistical averaging tends to cancel out phases.

We wrote a numerical ray-tracing code to study classical chaos where Snell's law is the physical principle used to determine the evolution of a ray, i.e.,

$$n_1 \sin(\theta_1) = n_2 \sin(\theta_2). \tag{3}$$

Here, n_1 and n_2 are the real parts of the index of the refraction of either side of an interface and θ_1 and θ_2 are the incident and refracted angles, respectively. Each ray is given an initial "intensity," $I_0 = 1$. There are three mechanisms that affect the intensity: reflection at and transmission through a boundary between two materials and absorption along the path of the ray, which we will model with the Beer-Lambert law. To calculate the intensity I, when a ray crosses an interface between different materials, we need reflection and transmission coefficients. The transverse electric (TE) Fresnel equations correspond to the case where the polarization of the electric field is perpendicular to the plane of incidence. For the one-dimensional case, there are no separate Fresnel equations for TE and transverse magnetic (TM). This is because the incoming ray vector coincides with the interface normal, and thus there is no plane of incidence. For the exact one-dimensional case,[49] there are no separate Fresnel equations for TE and TM. This is because the incoming ray vector coincides with the interface normal, and thus there is no plane of incidence. The reflection and transmission amplitudes of the transverse electric (TE) case are given by

$$r_{TE} = \frac{\cos\theta_1 - \sqrt{n'^2 - \sin^2\theta_1}}{\cos\theta_1 + \sqrt{n'^2 + \sin^2\theta_1}}, \tag{4}$$

$$t_{TE} = \frac{2\cos\theta_1}{\cos\theta_1 + \sqrt{n'^2 - \sin^2\theta_1}}, \tag{5}$$

where $n' = n_2/n_1$. The choice of using the TE Fresnel equations ensures that a scalar wave equation is exact when evaluating electromagnetic systems in two dimensions, or equivalently, three-dimensional systems with cylinder symmetry. The polarization of light does not change when it moves across an interface if the polarization is perpendicular to the plane of incidence. For later comparisons, our ray model was equipped with these specific Fresnel equations. These equations govern how much of the intensity is reflected and how much is transmitted. The corresponding reflection and transmission coefficients are

$$\mathcal{R} = |r_{TE}|^2, \tag{6}$$

$$\mathcal{T} = \frac{\sqrt{n'^2 - \sin^2\theta_1}}{\cos\theta_1} |t_{TE}|^2. \tag{7}$$

We consider materials with a small absorption coefficient n_i and, therefore, neglect the fact that absorption turns homogeneous into inhomogeneous plane waves in absorptive media.[50,51] Whenever Snell's law is referred to, it is the familiar law stated in Eq. (3).

Whenever a ray crosses an interface between two materials, it splits into a reflected ray and a transmitted ray. The practical implication of this is that calculations must be truncated because of run time. As long as we have splitting rays, there will be branches of the original ray that are inside the scatterer forever. We implemented a truncation condition that stops the simulation of a particular branch when $I_b < 10^{-5}$, where I_b is the intensity in that branch. The effect of the truncation threshold was thoroughly investigated by calculating the average intensity lost due to terminating the rays early, i.e., the truncation loss. For $n_{\text{dome}} \leq 2$, this value never exceeded 0.037% of the total average intensity. When $n_{\text{dome}} > 2$, the truncation loss was higher, but it never exceeded 0.74% of the total average intensity.

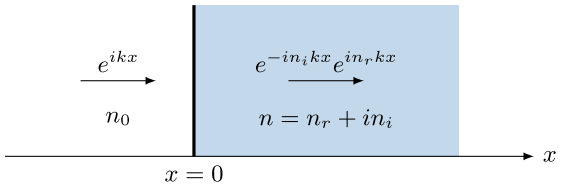

FIG. 2. A plane wave enters an absorbing material with a complex index of refraction $n = n_r + in_i$. The intensity of the wave decays exponentially with a factor of $e^{-4\pi n_i x/\lambda}$.

Whenever a ray splits, the intensity in the resulting two branches is determined according to the Fresnel coefficients stated in Eqs. (4) and (5). The subsequent absorption in the material is governed by the Beer-Lambert law explained in Sec. III B.

B. Beer-Lambert law of absorption

We use the Beer-Lambert law of absorption to provide an approximate measure of the absorption efficiency of our model, which we call the Beer-Lambert efficiency. It is an approximation because the classical ray model does not take diffraction into account as an electromagnetic simulation would do. The extinction coefficient in the Beer-Lambert law determines how fast the intensity of incoming radiation is decaying. Consider a plane wave e^{ikx}, incident on a slab of absorbing materials (see Fig. 2). Inside the material, the index of refraction, $n = n_r + in_i$, is complex, and the wave is

$$e^{inkx} = e^{i(n_r + in_i)kx} = e^{-n_i kx} e^{in_r kx}, \tag{8}$$

where $k = 2\pi/\lambda$ denotes the wave vector and x is the penetration-depth into the material. To obtain the intensity of the wave, we must take the absolute square value

$$\left|e^{-n_i kx} e^{in_r kx}\right|^2 = e^{-4\pi n_i x/\lambda}. \tag{9}$$

We now see that the intensity is decaying exponentially as a function of the path length inside of the absorbing material and the imaginary part of the refractive index of the material. In order to use our classical ray tracing approach, a transition from waves to rays is needed. We have chosen to assign each incoming ray an initial intensity of 1, which is reduced as a function of the path length only, since n_i is kept constant in the absorbing material.

IV. THE TRANSITION FROM REGULAR TO CHAOTIC DYNAMICS ENHANCES ABSORPTION EFFICIENCY

In this section, we discuss how the film + dome system transitions from regular to chaotic scattering dynamics and establish our central result, the correlation between the onset of chaos and the

rapid increase in the Beer-Lambert efficiency that systematically follows. We present results that show the transition from regular to chaotic dynamics in three different ways as a function of n_{dome}:

1. computation of the fractal dimension of the invariant set of infinitely long-lived trajectories;
2. the chaotic nature of Newtonian rays entering the system from the outside;
3. calculation of the absorption cross section, averaged over the wavelength in an electromagnetic simulation using a commercial finite-difference time-domain (FDTD) solver.[52]

To corroborate and confirm that the correlation between the onset of chaos and the enhancement of the Beer-Lambert efficiency is not specific to a certain special film thickness but a structurally stable phenomenon, we repeated the three routes we use to show the transition to chaos five times for varying film thicknesses. The only exceptions to this procedure are the electromagnetic simulations, which were studied only in the case of the 2 μm film. We start by showing the onset of chaos and its signatures for the system in Fig. 1(c), which has a 3.46 μm tall elliptical dome on top of a 2 μm thick film as an example, and end the section by showing the structural stability of the connection between the onset of chaos and the onset of absorption enhancement.

A. Scattering fractals and periodic orbits

A signature of chaos is the existence of chaotic repellers.[53] We, therefore, look for chaotic repellers in the invariant set of infinitely long-lived trajectories. We choose the bottom mirror of the bucket-shaped system as our PSOS and send nonabsorbing Newtonian rays from 10 080 equispaced positions in the spatial interval $x \in (0, 5)$, spanning the full width of the system, and from 10 080 equispaced angles in the interval $\theta \in (-\pi, \pi)$. The lifetime of these Newtonian rays is characterized by the number of collisions they make with the PSOS. This characterization ensures that a trapped ray may not simply live a long time in the scatterer, but has to return to the back mirror, thus spending a portion of its lifetime in the absorbing film, in order to be trapped. Rays with the initial angle π or $-\pi$ are omitted since they would bounce back and forth between the right and left mirrors forever. Figure 3 shows a visualization of the initial conditions of the rays, color-coded according to their lifetimes, ranging from deep blue for short lifetimes to yellow for long lifetimes, for four different indices of refraction of the dome. Since many subsets of these visualizations have fractal dimensions, we refer to these visualizations as scattering fractals. The horizontal axis of the scattering fractals corresponds to x, while the vertical axis corresponds to θ.

The lifetime of each ray is measured by the number of bounces it makes with the PSOS, in this case the rear mirror. The fractal dimension of each scattering fractal for n_{dome} between 1 and 2.5 in steps of 0.1 is found by the box counting method, see Fig. 7. In general, the transition to chaos may or may not be abrupt. In the case where it is not abrupt but gradual, more and more of the phase space will be chaotic during the transition. The film + dome system has a gradual transition to chaos. We have opted to define the onset of chaos in terms of n_{dome} as the cases where the calculated

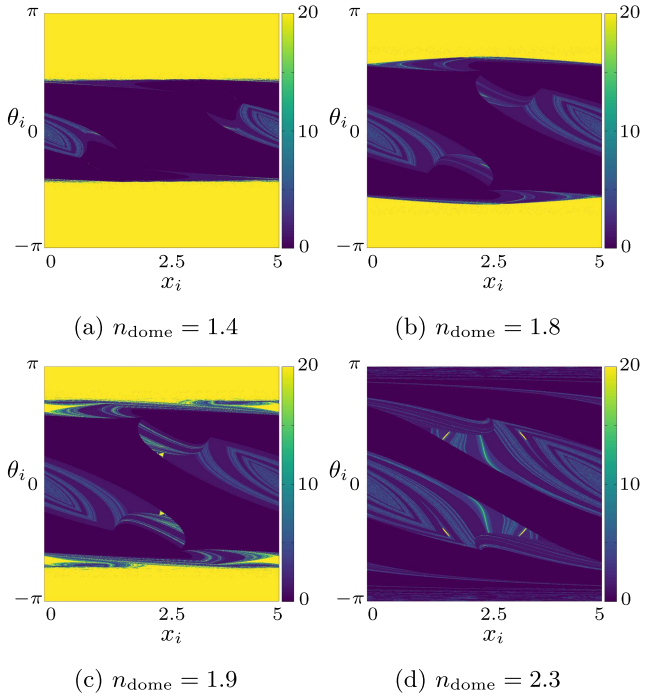

FIG. 3. Scattering fractals for four different film + dome systems for four different values of n_{dome}, respectively. In the case of (a), where $n_{\text{dome}} = 1.4$, the fractal dimension is $\simeq 2$. Hence, it is essentially a regular system. In (b) ($n_{\text{dome}} = 1.8$), (c) ($n_{\text{dome}} = 1.9$), and (d) ($n_{\text{dome}} = 2.3$), the fractal dimensions are less than the threshold value of 1.95. The scattering fractals show the lifetime in terms of the number of collisions with the PSOS. The initial angles, θ_i, and the initial positions, x_i, of the rays, cover the PSOS.

fractal dimension dropped below 1.95. In general, the scattering fractals will not behave as self-similar monofractals with simple scaling rules. The box-counting method was, therefore, used carefully and only on scattering fractals which did not exhibit multiple scaling rules. When computing scattering fractals for chaotic systems, one must also respect that the extreme sensitivity of chaos means that calculation precision can degrade quickly. The rays used for calculating fractal dimensions are cut off at 20 bounces on the PSOS to prevent this problem. This limit is the only truncation of the lifetime of the rays since absorption was turned off for the calculation of the scattering fractals. The example of the 2 μm thick film shows a fractal dimension below 1.95 when $n_{\text{dome}} \approx 1.5$, as indicated by the horizontal dashed line in Fig. 7(c).

When n_{dome} is exactly 1, it is equivalent to no dome at all, only the flat film, which must have fully regular dynamics. As expected, the fractal dimension is integer, $d = 2$. This is because rays started from the inside at shallow angles will be trapped forever due to the total internal reflection. There is a sharp transition from being trapped forever and escaping immediately in this case. When n_{dome} is increased, the geometry of the scattering fractal changes [Fig. 3(a)]. No longer is there a sharp transition between the trapped and the escaping rays. The border exhibits a fractal geometry and the lifetime of rays is

sensitive to the initial coordinate and angle. Further increase in n_{dome} yields an even more complex border where the lifetime of the rays is very sensitive to their initial conditions [Figs. 3(b) and 3(c)]. These complex borders are fractal, meaning that rays which enter the region near them might stay for a very long time in the system.[42]

When n_{dome} is increased beyond the index of refraction of the film, the invariant set gets drastically smaller [Fig. 3(d)]. The total internal reflection is now a possibility at the dome-film interface and thus rays are ejected from the chaotic repeller much earlier. Moreover, triangularlike regions of trapped rays start to appear in the scattering fractals for values of n_{dome} around 2 near the center of the scattering fractal. This can be seen as the small yellow regions in Figs. 3(c), 3(d), and 4(a), which shows an enlargement of the upper small yellow region in Fig. 3(c). To more clearly bring out the ray dynamics in the vicinity of the regular island shown in Fig. 4(a), Fig. 4(b) shows the phase-space portrait of rays that were sent out from the initial conditions of Fig. 4(a) and, to accurately represent the relatively long trajectories that linger in the vicinity of the regular island, the cut-off is now at 200 bounces instead of 20. The phase-space portrait in Fig. 4(b) shows a stable island surrounded by hyperbolas that close in on the three corners of the stable island. The orbit corresponding to the center of the stable island is shown in Fig. 4(c). This orbit is totally reflected at the air-dome interface. In the case of the total internal reflection, the full intensity of the ray is reflected, which is very beneficial from a light-trapping perspective. The fact that we are not looking to calculate the fractal dimension, but periodic orbits at this point, justifies the cut-off limit of 200 bounces on the bottom mirror. A ray launched from the initial condition pinched by the hyperbolas produces an orbit with period three, as seen in Figs. 4(d) and 4(e).

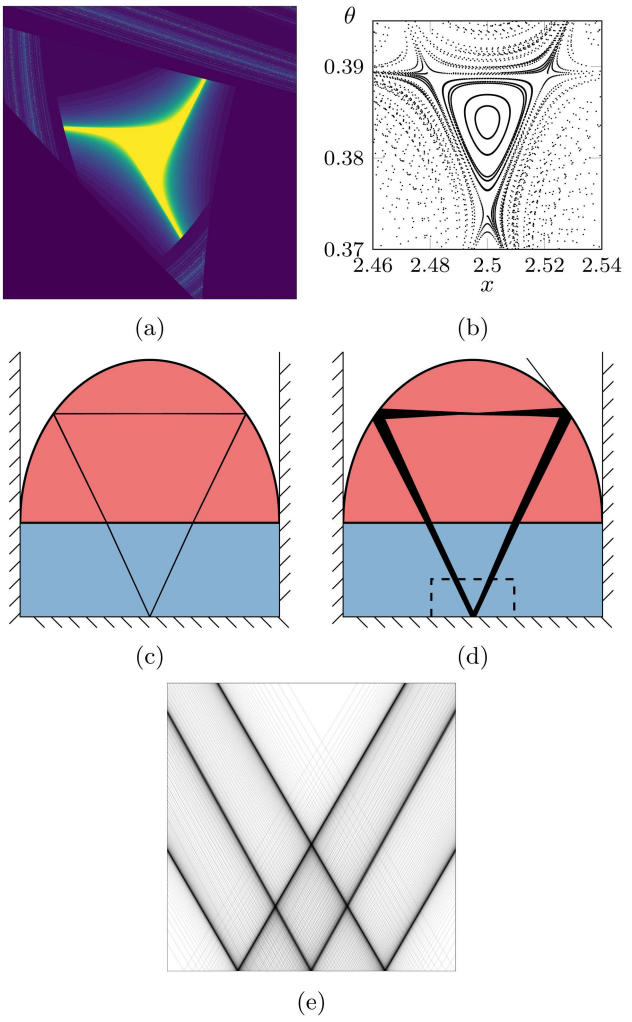

FIG. 4. (a) A chaotic repeller in the scattering fractal of the film + dome system for $n_{\text{dome}} = 1.9$. (b) The phase-space portrait generated by rays started for initial conditions in (a). (c) An orbit started near a fixed point. (d) An orbit started near a period three orbit. (e) A crop of the dashed area in (d) showing that the orbit is indeed a period three orbit.

B. Newtonian rays sent in from the outside

The onset of chaos can also be inferred from Newtonian rays sent in from the outside. When we model surface-structured solar cells with rays, we send the rays in straight down from the outside. Such rays behave very predictably for values of n_{dome} up to 1.65 as seen in Figs. 5(a) and 5(b). There is no sign of sensitivity with respect to the initial position above the film + dome system. In Figs. 5(c) and 5(d), we let $n_{\text{dome}} = 1.70$ and $n_{\text{dome}} = 1.75$, respectively, and we see that some of the rays start to take wildly different paths compared to their neighboring rays. This indicates the onset of chaos.

It is important to note that Fig. 5 shows Newtonian rays. Figure 5(a) does not show the trajectories of non-Newtonian rays, which are used for calculating the Beer-Lambert efficiency. The rays shown in Fig. 5(a) are Newtonian rays sent in from the outside. Despite the simplicity of this visualization, it captures the emergence of sensitivity to the initial positions of the rays.

Chaos in dynamical ray systems is often defined by a positive Lyapunov exponent. We calculated the Lyapunov exponent of Newtonian rays sent normally toward the dome-film interface from the outside. Figure 6 shows the Lyapunov exponents as a function of the initial starting positions, x_i, of the rays above the film + dome (2 μm thick film) system. Like in Fig. 5, we see a change when increasing n_{dome} beyond 1.65. At $n_{\text{dome}} = 1.7$, some of the rays exhibit a positive Lyapunov exponent. The number of rays with a positive Lyapunov exponent increases with n_{dome}. This result is consistent with the behavior of the scattering fractals and the results shown in Fig. 5.

C. Beer-Lambert efficiency

We simulate incoming sunlight by sending 5000 non-Newtonian rays in from the top as shown in Fig. 1(c) and average over the efficiency of each individual initial ray in order to calculate the Beer-Lambert efficiency. We chose to use $\lambda = 500$ nm in Eq. (9) for comparison with FDTD calculations, which will be presented in Sec. IV D. The initial conditions of the 5000 rays are evenly spread over the interval $x \in (0, 5)$. Since only the film is absorbing, the

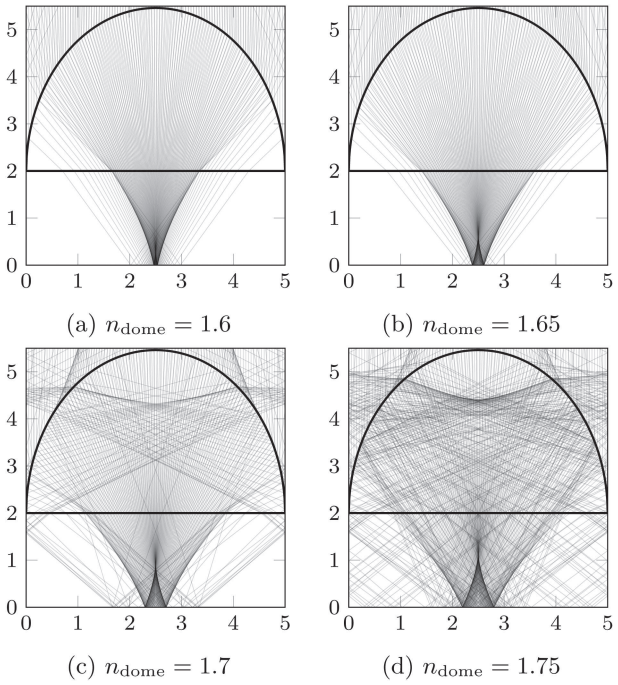

FIG. 5. Newtonian rays sent from the outside for different values of n_{dome}. At the breakpoint value $n_{\text{dome}} = 1.7$, the rays become sensitive to their initial condition.

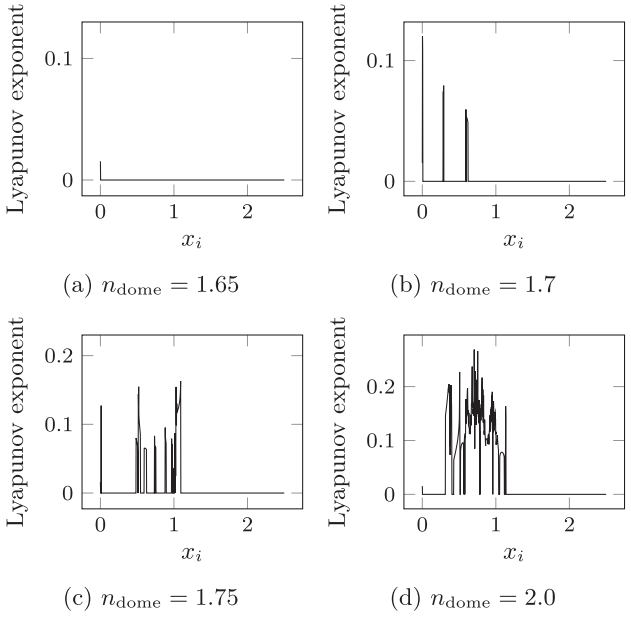

FIG. 6. Lyapunov exponents of Newtonian rays sent from the outside perpendicular with respect to the dome-film interface.

trajectories will have to spend a long time inside of it, not only in the dome structure, in order to deposit their intensity. This motivates the desire for long-lived trajectories, which could be provided by chaotic ray dynamics. Figure 7 shows that the Beer-Lambert efficiency increases monotonically as a function of n_{dome} before it falls off for $n_{\text{dome}} > 2.1$. Using the 2 μm thick film in Fig. 7(c) as an example, the increase in the Beer-Lambert efficiency starts slowly for $n_{\text{dome}} < 1.6$ and then increases rapidly after a critical value $n_{\text{dome}} = 1.6$. There is a systematic tendency of a slow increase for small values of n_{dome}, followed by a rapid increase at a critical value for all film thicknesses, although it is not so pronounced in the 0.5 μm thick film example, Fig. 7(a). The reason why the Beer-Lambert efficiency falls off at about $n_{\text{dome}} > 2.1$ is due to the total internal reflection at the dome-film interface, which prevents rays from coming back into the absorbing film. This effect starts at $n_{\text{dome}} \gtrsim 2$, but the real impact on the Beer-Lambert efficiency is when $n_{\text{dome}} > 2.1$. This effect is more dramatic for the thicker film examples because the path-length difference between a ray going straight down into the film and one coming in at an angle is greater than for a very thin film layer. At this point, the box counting method loses its usefulness. The invariant set is small and sparse, so the fractal dimension of the scattering fractal looks to be dependent on the scale. This is why there are no data points for the fractal dimension in Fig. 7 for $n_{\text{dome}} > 2.1$.

Both the fractal dimension and the Beer-Lambert efficiency are shown in Fig. 7. We see a striking correlation between the onset of chaos and the start of the rapid increase in the Beer-Lambert efficiency. The proposed explanation of this correlation is that the properties of chaotic scattering dynamics are beneficial for absorption efficiency modeled with the Beer-Lambert law because chaotic scattering, in conjunction with sticking to the chaotic repeller, leads to long trajectories inside of the absorbing film, which enhances the absorption. In addition, we demonstrated that chaos in the system leads to the spreading out of rays entering from the outside, a beneficial feature, which, again, leads to long trajectories with accompanying enhanced absorption, complex fractal boundaries in the invariant set as seen in the scattering fractals, which are "sticky," and the existence of stable periodic orbits. The most notable periodic orbit that was found is the period-three orbit, as shown in Fig. 4(b). It leads to "slow hyperbolic corners" in which the movement of the trajectories in the PSOS slows down tremendously [as seen from the closeness of successive points in Fig. 4(b)] as they approach, and ultimately round, the period-three corners of the stable islands.

It must be noted that the sole purpose of plotting the fractal dimension together with the Beer-Lambert efficiency in Fig. 7 is to show that the fractal dimension drops below the threshold value 1.95 for the same n_{dome} as the Beer-Lambert efficiency starts to increase more rapidly. There is no one-to-one relationship between the two quantities.

D. FDTD simulations of the electric field

The classical ray model that we presented provides us with an approximation of the amount of absorbed energy in a dielectric material. A real solar cell has complex physical processes that are not taken into account and take place starting from when light first enters the device, to the point when electric power is produced. Our model aims to predict and explain the efficiency enhancement due to light

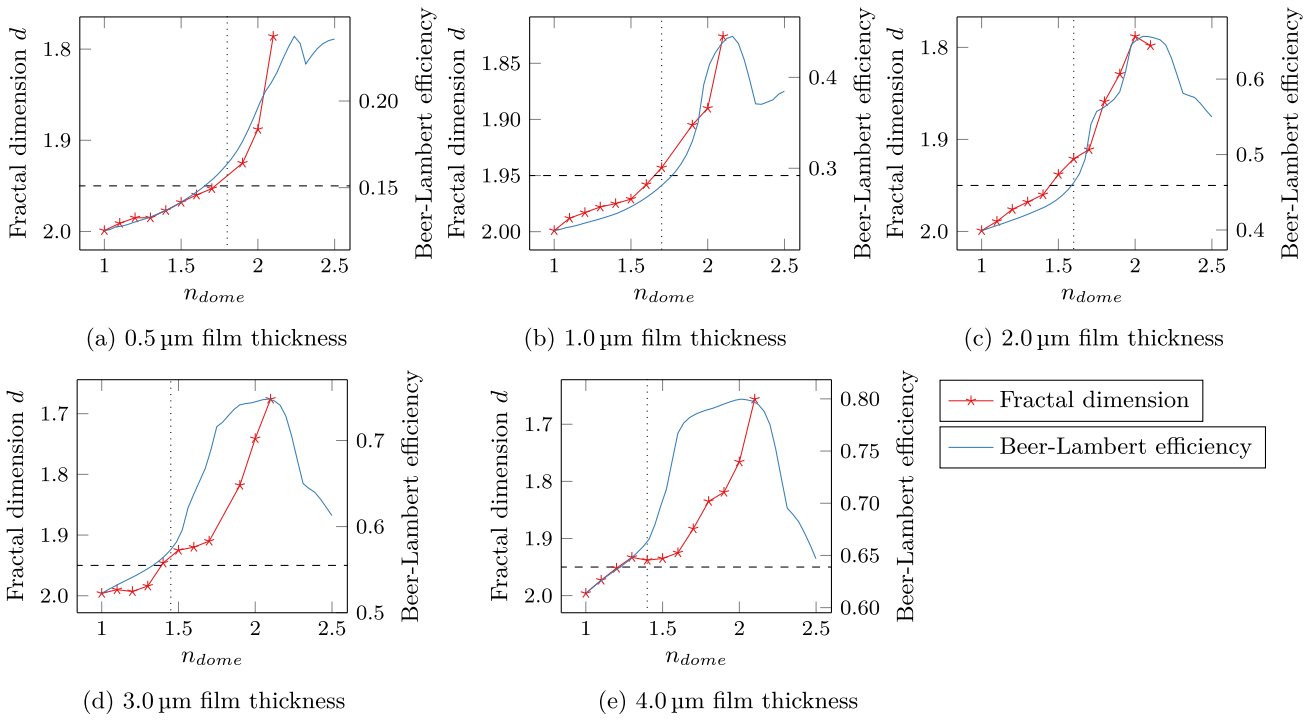

FIG. 7. Visualization of the fractal dimension (red) and the Beer-Lambert efficiency (blue). The onset of chaos is determined by the first data point below a fractal dimension of 1.95, indicated by a horizontal dashed line. The rapid increase of the Beer-Lambert efficiency is indicated by a vertical dotted line.

trapping, i.e., the increase in $1 - R$, on the basis of classical trajectory simulations. To prove that our ray-based results are relevant, we show here that full electromagnetic wave calculations, in the form of FDTD simulations of the film + dome system, corroborate what we have found in our classical simulations.

Our FDTD simulations are conducted in the following way. First, we chose our system, consisting of a dome of height 3.5 µm and an absorbing film of width 5 µm, a thickness of 2 µm, and a fixed index of refraction of $n_{\text{film}} = 2 + 0.0054i$. For this film + dome system, for each value of n_{dome} of a relatively dense set of n_{dome}

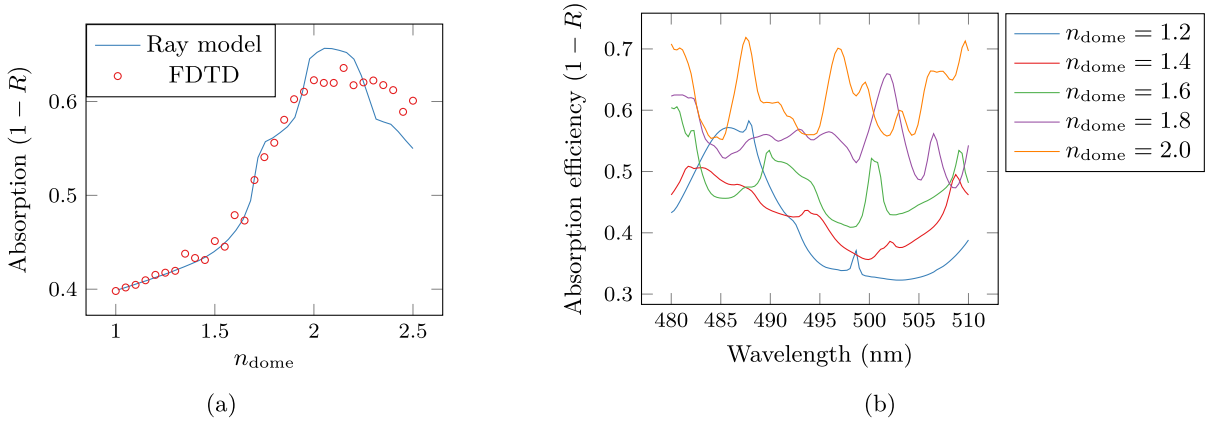

FIG. 8. (a) Absorption efficiency calculated with a commercial FDTD solver compared to the Beer-Lambert absorption efficiency calculated by rays. (b) Absorption efficiency as a function of wavelength calculated with FDTD for a range of n_{dome}. The number of resonances increases as n_{dome} increases.

values, ranging from $n_{\text{dome}} = 1$ in steps of $\Delta n_{\text{dome}} = 0.05$ to $n_{\text{dome}} = 2.5$, we computed the FDTD absorption value $1 - R$, and averaged $1 - R$ over wavelengths ranging from 480 nm in steps of 0.3 nm to 510 nm. The averaging mimics the fact that in practice solar cells are never irradiated with monochromatic light of a specific wavelength, but are irradiated with solar radiation, which is spread out over a range of wavelengths. As an additional, welcome benefit, the averaging smoothes over accidental wave resonances in our system, wave features that are clearly not present in our classical simulations. The result of our averaged FDTD simulations is shown in Fig. 8(a). We see that our classical simulations are very close to the full FDTD wave calculations, which shows that our classical ray simulations capture most of the (average) wave phenomena in our model solar cell. In addition, our FDTD simulations confirm the existence of the roughly three regions already presented and discussed in connection with Fig. 7, i.e., a slowly increasing region for $n_{\text{dome}} < 1.6$, a rapidly increasing region for $1.6 < n_{\text{dome}} < 2.1$, and a decreasing region for $n_{\text{dome}} > 2.1$. We explain the good agreement between the full-E&M FDTD calculations and our classical simulations on the basis that the wavelength of the incoming light is much smaller than the system size. Therefore, the classical ray model approximates the full E&M wave solution very well, as seen in Fig. 8(a). While, as mentioned in Sec. III A, complete agreement between classical and wave calculations can be expected only if the classical rays are properly equipped with phases, which are neglected in our classical simulations, the averaging of our FDTD results over different wavelengths clearly contributes to de-emphasize the importance of phases, an expected result according to our discussion in Sec. III A.

For some selected values of n_{dome}, Fig. 8(b) shows the FDTD-computed resonance structures in the absorption $1 - R$ as a function of wavelength that we averaged over in Fig. 8(a). As the value of n_{dome} increases, the number of resonances in the selected frequency interval is seen to increase. This is easily understood on the basis that, for increasing n_{dome}, the effective wavelength inside of the dome material becomes shorter ($\lambda_{\text{dome}} = \lambda_{\text{vacuum}}/n_{\text{dome}}$), allowing more resonances to exist inside the fixed dome geometry.

An additional corroboration for the chaos transition at $n_{\text{dome}} \sim 1.5$ can be obtained by directly inspecting the wavefunctions in the film + dome system. To this end, we used the FDTD solver to compute the absolute square value, $|\mathbf{E}|^2$, of the electric field, for four different values of n_{dome} (see Fig. 9). For small values of n_{dome} [Figs. 9(a) and 9(b)], the electric field behaves predictably. We see that, reminiscent of the behavior of the rays shown in Fig. 5, the dome is focusing the incoming light into the absorbing film, where a plane-wavelike resonance forms. For larger values of n_{dome} [see Figs. 9(c) and 9(d)], we see a distinct qualitative difference in the structure of $|\mathbf{E}|^2$, showing complex wave patterns and so-called scarlets[54] that are a signature of chaos. In addition, whenever there is a transition from regular to chaotic dynamics, it is expected that at the transition to chaos the electric field starts to spread out over the entire available scattering volume. This phenomenon can, to some degree, also be seen directly in the $|\mathbf{E}|^2$ patterns in Fig. 9.

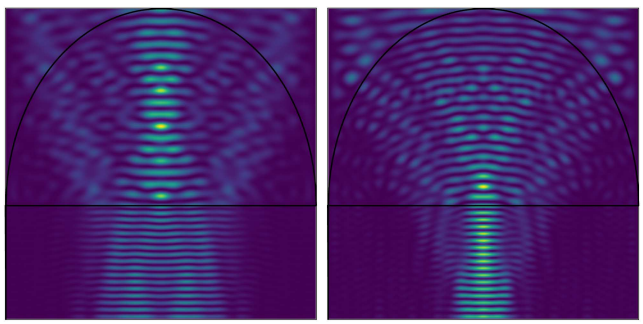

(a) Regular, $n_{\text{dome}} = 1.2$ (b) Regular, $n_{\text{dome}} = 1.4$

(c) Chaotic, $n_{\text{dome}} = 1.8$ (d) Chaotic, $n_{\text{dome}} = 2.0$

FIG. 9. FDTD simulations of the electric field inside the film + dome system for several values of n_{dome}. The black-line overlays show the shape of the film + dome system. The colors are chosen for the sole purpose of making clear visuals and to bring out the patterns in the electric field. Thus, the assignment of colors to electric field intensities is not necessarily the same for all four frames. Since only the structure of the field is of interest here, not the specifics of the intensities, color bars that would reflect the assignments of electric field intensities to colors are omitted.

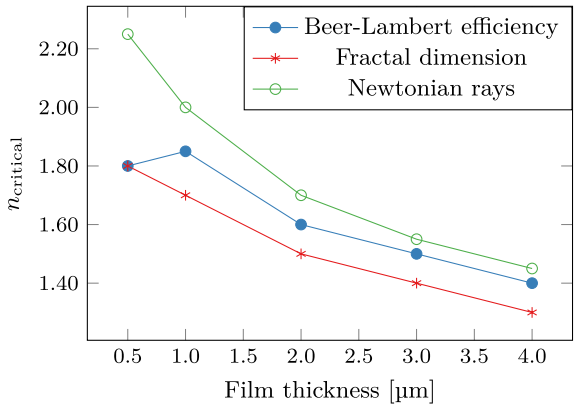

FIG. 10. The n_{critical} is the value for when the Beer-Lambert efficiency (blue) starts to increase more rapidly, the fractal dimension (red) is below 1.95, and the Newtonian rays sent from the outside directly downwards (green) visually start to behave sensitively on the initial condition. n_{critical} can be directly read off from Figs. 5 and 7. The lines between the dots are there to guide the eyes.

E. Structural stability

In Fig. 10, we summarize our results across the five film + dome systems we investigated, where film thickness was the independent parameter. The onset of chaos has been determined from the fractal dimension of the scattering fractals (see Fig. 7) and from visually inspecting the sensitivity of Newtonian rays to their initial conditions (see Fig. 5). There is a clear trend that shows that the onset of chaos correlates with the onset of the rapid enhancement of the Beer-Lambert efficiency.

V. CONCLUSION

We have evaluated absorption enhancement in a scattering system exhibiting a transition between regular and chaotic classical dynamics. The model system mimics a structured solar cell and was obtained by placing an elliptical dome structure on top of a flat absorbing film. A classical ray-tracing code was developed for modeling surface-structured optically thin solar cells. The Beer-Lambert law was used to model the absorption of light in the dielectric material.

We found that increasing the index of refraction inside the dome structure leads to a transition of the system from one that scatters regularly, to one with chaotic scattering dynamics. The scattering dynamics was investigated by calculating Lyapunov exponents and the fractal dimension of scattering fractals. We demonstrate that this transition from regular to chaotic dynamics goes along with an enhancement of the absorption efficiency in the film. Enhancing absorption efficiency by surface structuring is not new and is already well documented. However, in this paper, we have demonstrated that the onset of chaotic scattering dynamics is clearly correlated with absorption enhancement.

We, therefore, suggest to actively use the mechanism of chaos in the design of surface structures for solar cells. The classical ray model approximation presented in this paper represents one strategy for the establishment of a connection between chaotic scattering and absorption enhancement. It allows one to exploit this connection as a powerful guide for designing surface structures with a very high light-trapping efficiency for use in optically thin solar cells.

ACKNOWLEDGMENTS

This work was supported by the grant "Development of a new ray model for understanding the coupling between dielectric spheres for photovoltaics with higher efficiency" (No. 250678) financed by The Research Council of Norway. High-performance computing resources were provided by UNINETT Sigma2 through Grant No. NN9516K.

REFERENCES

[1] T. Tiedje, E. Yablonovitch, G. D. Cody, and B. G. Brooks, "Limiting efficiency of silicon solar cells," IEEE. Trans. Electron Dev. **31**, 711–716 (1984).
[2] H. A. Atwater and A. Polman, "Plasmonics for improved photovoltaic devices," Nat. Mater. **9**, 205 (2010).
[3] J. Gjessing, E. S. Marstein, and A. Sudbø, "2D back-side diffraction grating for improved light trapping in thin silicon solar cells," Opt. Express **18**, 5481–5495 (2010).
[4] J. Gjessing, A. Sudbø, and E. Marstein, "A novel back-side light-trapping structure for thin silicon solar cells," J. Eur. Opt. Soc. Rapid Publ. **6**, 11020 (2011).
[5] C. Battaglia, C.-M. Hsu, K. Söderström, J. Escarré, F.-J. Haug, M. Charriére, M. Boccard, M. Despeisse, D. T. L. Alexander, M. Cantoni, Y. Cui, and C. Ballif, "Light trapping in solar cells: Can periodic beat random?," ACS Nano **6**, 2790–2797 (2012).
[6] P. Kowalczewski, M. Liscidini, and L. C. Andreani, "Light trapping in thin-film solar cells with randomly rough and hybrid textures," Opt. Express **21**, A808–A820 (2013).
[7] Q. Tang, H. Shen, H. Yao, K. Gao, Y. Jiang, Y. Li, Y. Liu, L. Zhang, Z. Ni, and Q. Wei, "Superiority of random inverted nanopyramid as efficient light trapping structure in ultrathin flexible c-Si solar cell," Renew. Energy **133**, 883–892 (2019).
[8] Y. Xu and Y. Xuan, "Photon management of full-spectrum solar energy through integrated honeycomb/cone nanostructures," Opt. Commun. **430**, 440–449 (2019).
[9] J. Grandidier, D. M. Callahan, J. N. Munday, and H. A. Atwater, "Light absorption enhancement in thin-film solar cells using whispering gallery modes in dielectric nanospheres," Adv. Mater. **23**, 1272–1276 (2011).
[10] E. Yablonovitch, "Statistical ray optics," J. Opt. Soc. Am. **72**, 899–907 (1982).
[11] F. Haake, *Quantum Signatures of Chaos*, 3rd ed. (Springer, Berlin, 2010).
[12] H.-J. Stöckmann, *Quantum Chaos: An Introduction* (Cambridge University Press, Cambridge, 2000).
[13] M. C. Gutzwiller, *Chaos in Classical and Quantum Mechanics* (Springer, New York, 1990).
[14] H. Poincaré, "Introduction," Acta Math. **13**, 5–7 (1890).
[15] E. N. Lorenz, "Deterministic nonperiodic flow," J. Atmos. Sci. **20**, 130–141 (1963).
[16] J. Hadamard, "Les surfaces á courbures opposées et leurs lignes géodésiques," J. Math. Pures Appl. **4**, 27–74 (1898).
[17] L. A. Bunimovich, "On the ergodic properties of nowhere dispersing billiards," Commun. Math. Phys. **65**, 295–312 (1979).
[18] L. A. Bunimovich, "On ergodic properties of certain billiards," Funct. Anal. Appl. **8**, 254–255 (1974).
[19] L. A. Bunimovich, "Decay of correlations in dynamical systems with chaotic behavior," Zh. Eksp. Teor. Fiz. **89**, 1452–1471 (1985).
[20] H. Cao and J. Wiersig, "Dielectric microcavities: Model systems for wave chaos and non-Hermitian physics," Rev. Mod. Phys. **87**, 61–111 (2015).
[21] E. G. Altmann, J. S. E. Portela, and T. Tél, "Leaking chaotic systems," Rev. Mod. Phys. **85**, 869–918 (2013).
[22] L. Sirko, P. M. Koch, and R. Blúmel, "Experimental identification of non-Newtonian orbits produced by ray splitting in a dielectric-loaded microwave cavity," Phys. Rev. Lett. **78**, 2940–2943 (1997).
[23] E. Ott and T. Tél, "Chaotic scattering: An introduction," Chaos **3**, 417–426 (1993).
[24] P. Gaspard and S. A. Rice, "Scattering from a classically chaotic repellor," J. Chem. Phys. **90**, 2225–2241 (1989).
[25] J. Hietarinta and S. Mikkola, "Chaos in the one-dimensional gravitational three-body problem," Chaos **3**, 183–203 (1993).
[26] P. T. Boyd and S. L. W. McMillan, "Chaotic scattering in the gravitational three-body problem," Chaos **3**, 507–523 (1993).
[27] A. A. Chernikov and G. Schmidt, "Chaotic scattering and acceleration of particles by waves," Chaos **3**, 525–528 (1993).
[28] K. Richter and D. Wintgen, "Analysis of classical motion on the Wannier ridge," J. Phys.: At. Mol. Opt. Phys. **23**, L197–L201 (1990).
[29] T. Yamamoto and K. Kaneko, "Helium atom as a classical three-body problem," Phys. Rev. Lett. **70**, 1928–1931 (1993).
[30] C. F. Hillermeier, R. Blümel, and U. Smilansky, "Ionization of H Rydberg atoms: Fractals and power-law decay," Phys. Rev. A **45**, 3486–3502 (1992).
[31] J. M. Seoane and M. A. F. Sanjuán, "New developments in classical chaotic scattering," Rep. Progress Phys. **76**, 016001 (2012).
[32] A. Kohler and R. Blümel, "Annular ray-splitting billiard," Phys. Lett. A **238**, 271–277 (1998).
[33] A. Kohler and R. Blümel, "Signature of periodic lateral-ray orbits in a rectangular ray-splitting billiard," Phys. Lett. A **247**, 87–92 (1998).

[34]A. Kohler and R. Bümel, "Test of semiclassical amplitudes for quantum ray-splitting systems," Phys. Rev. E **59**, 7228–7230 (1999).
[35]A. Kohler, G. H. M. Killesreiter, and R. Bümel, "Ray splitting in a class of chaotic triangular step billiards," Phys. Rev. E **56**, 2691–2701 (1997).
[36]A. Kohler and R. Blümel, "Weyl formulas for quantum ray-splitting billiards," Ann. Phys. **267**, 249–280 (1998).
[37]N. Savytskyy, A. Kohler, S. Bauch, R. Bümel, and L. Sirko, "Parametric correlations of the energy levels of ray-splitting billiards," Phys. Rev. E **64**, 036211 (2001).
[38]Y. Hlushchuk, A. Kohler, S. Bauch, L. Sirko, R. Bümel, M. Barth, and H.-J. Stöckmann, "Autocorrelation function of level velocities for ray-splitting billiards," Phys. Rev. E **61**, 366–370 (2000).
[39]M. Mariano, G. Kozyreff, L. G. Gerling, P. Romero-Gomez, J. Puigdollers, J. Bravo-Abad, and J. Martorell, "Intermittent chaos for ergodic light trapping in a photonic fiber plate," Light Sci Appl. **5**, e16216 (2016).
[40]R. Blümel and W. P. Reinhardt, *Chaos in Atomic Physics* (Cambridge University Press, 1997).
[41]P. Cvitanović, R. Artuso, R. Mainieri, G. Tanner, and G. Vattay, *Chaos: Classical and Quantum* (Niels Bohr Institute, Copenhagen, 2016).
[42]L. P. Kadanoff and C. Tang, "Escape from strange repellers," Proc. Natl. Acad. Sci. U.S.A. **81**, 1276–1279 (1984).
[43]B. Mandelbrot, "How long is the Coast of Britain? Statistical self-similarity and fractional dimension," Science **156**, 636–638 (1967), see http://science.sciencemag.org/content/156/3775/636.full.pdf.
[44]B. Klinkenberg, "A review of methods used to determine the fractal dimension of linear features," Math. Geol. **26**, 23–46 (1994).
[45]T. Smith, G. Lange, and W. Marks, "Fractal methods and results in cellular morphology—Dimensions, lacunarity and multifractals," J. Neurosci. Methods **69**, 123–136 (1996).
[46]A. Kohler, G. H. M. Killesreiter, and R. Blümel, "Ray splitting in a class of chaotic triangular step billiards," Phys. Rev. E **56**, 2691–2701 (1997).
[47]A. Kohler, "Classical and quantum implications of ray splitting," Ph.D. thesis (Albert-Ludwigs-Universität Freiburg i.Br., 1998).
[48]M. A. Green, "Self-consistent optical parameters of intrinsic silicon at 300 K including temperature coefficients," Solar Energy Mater. Solar Cells **92**, 1305–1310 (2008).
[49]M. Brandsrud, E. Seim, R. Lukacs, A. Kohler, E. Marstein, E. Olsen, and R. Blümel, "Exact ray theory for the calculation of the optical generation rate in optically thin solar cells," Physica E **105**, 125–138 (2019).
[50]P. C. Chang, J. Walker, and K. Hopcraft, "Ray tracing in absorbing media," J. Q. Spectrosc. Radiat. Transf. **96**, 327–341 (2005).
[51]M. A. Dupertuis, M. Proctor, and B. Acklin, "Generalization of complex Snell–Descartes and Fresnel laws," J. Opt. Soc. Am. A **11**, 1159–1166 (1994).
[52]Lumerical Inc., see lumerical.com for "FDTD Solutions" (2019).
[53]E. Ott, *Chaos in Dynamical Systems* (Cambridge University Press, Cambridge, 1993).
[54]E. J. Heller, "Bound-state eigenfunctions of classically chaotic Hamiltonian systems: Scars of periodic orbits," Phys. Rev. Lett. **53**, 1515–1518 (1984).